Progress In Electromagnetics Research B, Vol. 57, 63–73, 2014

Passive Millimeter Wave Image Denoising Based on Adaptive Manifolds

Shujin Zhu [1], Yuehua Li [1,*], Jianfei Chen [1], and Yuanjiang Li [1, 2]

Abstract—Since the characters of poor inherent resolution and low signal-to-noise limit the application of the passive millimeter wave (PMMW) image, it is particularly important to improve the resolution and denoise the PMMW image. In this paper, the adaptive manifolds filtering algorithm based on non-local means (AM-NLM) is illustrated in detail. And an improved version of AM-NLM filtering algorithm is proposed for processing the PMMW image. The proposed algorithm firstly applies the AM-NLM filtering to obtain the basic denoised PMMW image. Then the image enhancement based on Laplacian of Gaussian operator is performed to enhance the edge of the target in PMMW image. Finally, the hard-threshold filtering with different thresholds is adopted to filter each dimension to achieve the final filtering response. Experimental results have shown that the proposed PMMW filtering algorithm has better and more satisfactory performance compared to AM-NLM, both in subjective visual effect and objective image quality metric. Additionally, our proposed algorithm is also available for real PMMW images.

1. INTRODUCTION

PMMW imaging has numerous advantages over infa-red (IR) and optical imaging by being able to work well under complex and adverse environment. PMMW has been widely used in earth remote sensing, radio astronomy, cosmology, air sounding, and commercial applications [1]. For instance, during the imaging of earth remote sensing, PMMW imaging system can pass through the cloud layer and dust to achieve the image of the ground; during the forest fire detection it is also capable to detect the fire source which is optically masked by obstacles [2]. Synthetic aperture imaging radiometer (SAIR), which employs a number of identical antennas and receivers distributed in space to form sparse array, can attain desirable spatial resolutions without scanning system [3]. Although the PMMW imaging provides a lot of benefits compared to IR and optical imaging, there are several disadvantages. Due to existence of the partial coherence between targets, the differences of antenna or lens position and other imaging mechanism, the original PMMW image acquired from practical sensing operations is usually seriously noised, low resolution and blurry compared to optical and infrared images.

The fundamental principle underlying the sensing operation is the low-pass filtering due to the antenna lens' finite size and also, the output image of the imaging system is a low-pass filtered version of the original scene [4]. There is no useful signal beyond the cut-off frequency in the measured data and the detail target information in the scene is submerged by noise in the produced PMMW image. Thus PMMW image super-resolution technology grows inevitably important as the development of PMMW imaging technology. Summarily image processing can be sorted into two levels: denoising, to filter random elements unrelated to target in image, it usually does not consider point spread function (PSF); deconvolution or super-resolution, to remove system impact, it generally refers to restore inhibited frequency components above cut-off frequency by analytical continuation in frequency domain, to expand image spectrum, so as to achieve interpolation in space domain, furthermore breakthrough

Received 26 September 2013, Accepted 18 November 2013, Scheduled 22 November 2013

* Corresponding author: Yuehua Li (nlglyh2013@sina.cn).

[1] School of Electronic Engineering and Optoelectronic Technology, Nanjing University of Science and Technology, Nanjing 210094, China. [2]Institute of Electronic and Information, Jiangsu University of Science and Technology, Zhenjiang 212000, China.

to Rayleigh limit [5, 6]. Super-resolution algorithms can be classified into iterative and non-iterative algorithms. Iterative algorithms are generally the preferred approach due to their numerous advantages and also since the iteration can be terminated once a solution of a reasonable quality is achieved [7].

Some PMMW image super-resolution algorithms have been already proposed including: Lucy-Richardson algorithm [8, 9], MAP algorithm [10], conjugate gradients [11] and projection on convex set (POCS) method [12]. Wang resumes restoration of hidden target PMMW images by taking the estimated PSF into restoration algorithm based on maximum likelihood (ML) estimation and blind deconvolution techniques [5]. In paper [13], the authors apply Fourier-wavelet regularized deconvolution which exploits the Fourier domain representation of the convolution operator and the spatially adaptive wavelet domain representation of the signal to restore the PMMW image. And a PMMW image denoising method based on adaptive sparse representation with a learned overcomplete dictionary is proposed by Zhang in [14]. Recently, the adaptive manifolds filtering algorithm based on non-local means technology (AM-NLM) is proposed in paper [15] which has been proved flexible and effective. And we found that the AM-NLM filtering algorithm also works for PMMW images but cannot wipe off noise around target completely. In this paper, an improved version of AM-NLM is proposed for processing the simulated PMMW images by using Laplacian of Gaussian operator based enhancement and hard-threshold filtering in each dimension. Experiments are given to show that the proposed method can greatly improve the quality of PMMW image and avoid introducing blur to it.

2. ADAPTIVE MANIFOLDS FILTERING ALGORITHMS

2.1. Adaptive Manifolds Filtering Algorithm Based on Non-local Means

AM-NLM is the first high-dimensional filter for performing high-dimensional filtering of images and videos in real time which is quite flexible, capable of producing responses that approximate either standard Gaussian, bilateral, or non-local-means filters. The flowchart of AM-NLM filtering algorithm is illustrated in Figure 1.

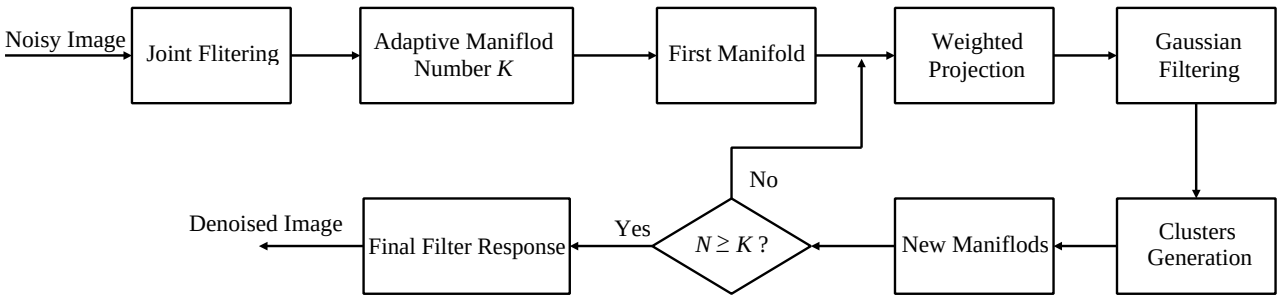

Figure 1. Flowchart of AM-NLM filtering algorithm.

Let $f : S \subset \mathbb{R}^{d_S} \rightarrow R \subset \mathbb{R}^{d_R}$ be a signal associating each point from its d_S-dimensional spatial domain S to a value in its d_R-dimensional range R. For grayscale images, $d_S = 2$ and $d_R = 1$, while for RGB color images $d_S = 2$ and $d_R = 3$.

Given a noisy image with N pixels, a set of high-dimensional image data can be created by performing joint filtering to the input image f [15]. Then, the number of manifolds K which is independent of the filter dimensionality is computed with the function:

$$K = 2 + \max(2, [H_S L_R]) \tag{1}$$

where H_S is a height computed from the spatial standard deviation of the filter, and L_R is a linear correction computed from the range standard deviation:

$$\begin{aligned} H_S &= \left[\log_2\left(\sqrt{\max(\Sigma_S)}\right)\right] - 1 \\ L_R &= 1 - \sqrt{\min(\Sigma_R)} \end{aligned} \tag{2}$$

By locally averaging pixel values to the created high-dimensional image data and performing low-pass filtering, adaptive manifolds can be obtained and are guaranteed to be approximately linear in all local neighborhoods [7]. The k-th d_S-dimensional adaptive manifold can be described by a graph (p_i, η_{ki}), and the manifold value $\eta_{ki} \in R$ associated with pixel $p_i \in S$ is defined by the evaluation of a function $\eta_k : S \to R$ at $p_i : \eta_{ki} = \eta_{ki}(p_i)$. The first manifold can be computed by low-pass filtering the input signal:

$$\eta_1(p_i) = (h_{\Sigma_S} * f)(p_i) \tag{3}$$

where $*$ is convolution, and h_{Σ_S} is a low-pass filter in S with covariance matrix Σ_S.

After the first manifold η_1 is generated, perform a Gaussian distance-weighted projection of all pixels p_i onto the manifold. The sampling points $\hat{\eta}_{ki}$ store the values of projection:

$$\Psi_1(\hat{\eta}_{ki}) = \phi_{\frac{\Sigma_R}{2}}(\eta_{ki} - f_i)f_i \tag{4}$$

Perform Gaussian filtering over each manifold mixing the values Ψ_1 from all sampling points $\hat{\eta}_{ki}$ to obtain the blurred values $\Psi_2(\hat{\eta}_{ki})$.

$$\Psi_2(\hat{\eta}_{ki}) = \sum_{p_j \in S} \phi_{\Sigma_\eta}(\hat{\eta}_{ki} - \hat{p}_j)f_j, \quad \Sigma_\eta = \begin{bmatrix} \Sigma_S & 0 \\ 0 & \Sigma_R/2 \end{bmatrix} \tag{5}$$

where $\hat{p}_j = (p_j, f_j)$, Ψ_2 defines a Gaussian filtering (a convolution) on a d-dimensional space.

Then, according to the direction v_1 that describes the variations of pixel about manifold η_1, pixels are divided into two clusters C_- (locally 'above') and C_+ (locally 'below'). Then a new manifold is computed as follows:

$$\eta_-(p_i) = \sum_{p_j \in C_-}^{N} W_-(p_j)f_j \Big/ \sum_{p_j \in C_-}^{N} W_-(p_j) \tag{6}$$

$$W_-(p_j) = \theta(\eta_{1j} - f_j)h_{\Sigma_S}(p_i - p_j) \tag{7}$$

h_{Σ_S} is the low-pass filter used to generate η_1, and θ is a weight function that gives more weight to pixels p_j not well represented by the manifold η_1:

$$\theta(\eta_{1j} - f_j) = 1 - \phi_{\frac{\Sigma_R}{2}}(\eta_{1j} - f_j) \tag{8}$$

where f_j is the color of pixel p_j. The manifold η_+ is generated similarly as above.

Whether more manifolds are needed is then decided by comparing the current number of manifolds to the needed number of manifolds K. If the number of manifolds is insufficient, new manifolds η_{--}, η_{-+} and η_{+-}, η_{++} with η_-, C_- and η_+, C_+ respectively will be generated.

After all needed manifolds are generated, the final filter response g_i for each pixel is computed by interpolating blurred values Ψ_2 gathered from all adaptive manifolds:

$$g_i = \frac{\sum_{k=1}^{K} w_{ki}\Psi_2(\hat{\eta}_{ki})}{\sum_{k=1}^{K} w_{ki}\Psi_2^0(\hat{\eta}_{ki})}, \quad w_{ki} = \phi_{\frac{\Sigma_R}{2}}(\eta_{ki} - f_i) \tag{9}$$

where $\Psi_2^0(\hat{\eta}_{ki})$ is the blurred version of $\Psi_1^0(\hat{\eta}_{ki})$:

$$\Psi_1^0(\hat{\eta}_{ki}) = \phi_{\frac{\Sigma_R}{2}}(\eta_{ki} - f_i) \tag{10}$$

2.2. Millimeter Wave Image Denoising Based on Adaptive Manifolds

It is true that the AM-NLM filtering algorithm does perform an excellent filtering result for the general images. But for the special PMMW image, whether the AM-NLM is effective has not been proved in the previous researches. In this section, AM-NLM filtering algorithm is tested to denoise our PMMW image, and it is found workable when processing PMMW image. However, the AM-NLM denoised result is a little blurry, and the noise around the target is still retained. Thus, an improved version of AM-NLM is proposed by using Laplacian of Gaussian operator based enhancement and hard-threshold filtering in each dimension to restore the PMMW image.

The PMMW image filtering algorithm proposed in this paper firstly applies joint filtering to create a set of high-dimensional PMMW image data $f_{out,i}$ with the input PMMW image f_i, in which $f_{out,i}$ is $(2 \times r + 1)^2 \times 3$ dimensions if the patch radius is set as r for RGB image [15]:

$$f_{out,i} = \sum_{p_j \in S} \phi(P_i - P_j) f_j \Big/ \sum_{p_j \in S} \phi(P_i - P_j) \tag{11}$$

where $P_i = (p_{i1}, p_{i2}, \ldots, p_{in})$, $n = (2 \times r + 1)^2$ is the i-th pixel p_i ($p_i = (x_i, y_i)$) centered patch and ϕ is an axis-aligned Gaussian function:

$$\phi_\Sigma(P_i - P_j) = \exp\left(-\frac{1}{2}(P_i - P_j)^T (P_i - P_j)\right) \tag{12}$$

where Σ is a $d \times d$ diagonal covariance matrix that controls how fast the weights decrease with distance, and $(P_i - P_j)^T$ is the transpose of matrix.

Perform AM-NLM filtering to high-dimensional PMMW image data to obtain the basic filtering result $g_{\text{AM-NLM}}$.

As the edge of target in the basic denoised image is still blurry, and some serious noise points have not been removed completely, the image enhancement algorithm based on Laplacian of Gaussian operator is applied:

$$g_{\log,i} = g_{\text{AM-NLM},i} + g_{\text{AM-NLM},i} * \nabla^2 G_i \tag{13}$$

$\nabla^2 G_i$ is the Laplacian of Gaussian operator:

$$\nabla^2 G_i = \frac{\partial^2 G_i}{\partial x_i^2} + \frac{\partial^2 G_i}{\partial y_i^2} = \frac{-1}{2\pi\sigma^4}\left(2 - \frac{x_i^2 + y_i^2}{\sigma^2}\right) e^{-\frac{x_i^2 + y_i^2}{\sigma^2}} \tag{14}$$

The image enhancement algorithm based on Laplacian of Gaussian operator indeed enhances the edge of target. However, the noise associated with the edge enhancement is also strengthened. Thus, perform hard-threshold filtering to each dimension to denoise the enhancement PMMW image to achieve the final filtering response $g_{k,i}$:

$$g_{k,i} = \begin{cases} g_{\log,i}, & |g_{\log,i}| \geq \delta_k \\ 0, & |g_{\log,i}| < \delta_k \end{cases} \tag{15}$$

where δ_k is the adopted threshold of hard-threshold filter in each dimension. For grayscale images, g_i is deemed as the final filtering response. $g_{1,i}$, $g_{2,i}$ and $g_{3,i}$ can be gained for color images as the three color channels.

The steps of the proposed algorithm in this paper can be concluded as follows:

1) Generate a set of high-dimensional PMMW image data $f_{out,i}$ by joint filtering.
2) Perform adaptive manifolds filtering algorithm based on non-local means to high-dimensional PMMW image data $f_{out,i}$ to gain the basic filtering image $g_{\text{AM-NLM}}$.
3) Apply image enhancement algorithm based on Laplacian of Gaussian operator to enhance the target edge in image $g_{\text{AM-NLM}}$.
4) The hard-threshold filtering to each dimension is adopted to further denoise the remaining noise. By selecting suitable threshold, a satisfied result $g_{final,i}$ can be reached.

2.3. The Analysis of Detail Implementation of Proposed PMMW Image Filtering Algorithm

Our proposed PMMW image filtering algorithm applies AM-NLM filtering to denoise high dimension image data and image enhancement algorithm based on Laplacian of Gaussian is adopted to enhance the target edge. Finally the background and useless noise information are filtered with hard-threshold filtering on each dimension. In this section, the analysis of the implementation of proposed algorithm will be discussed.

As it has been proved, using 6 PCA-computed main dimensions can actually produce better denoising results than working with the full space by Tasdizen in paper [16]. Thus, to make the

result convictive, we use this rule with the default parameter defined in [15] when applying AM-NLM filtering algorithm. The first several dimensions of image data are shown in Figure 2.

It is shown that the first dimensional image retains most information of the PMMW image, and as the increase of the dimension the image retains less information than previous one which can demonstrate the validity of the rule in [16].

Since the spherical wave has serious influence on near range millimeter wave radiometer imaging, the bright temperature of imaging result has big error [17]. Thus the structural similarity index measurement (SSIM) [18] which measures the similarity between two images is used as the main objective image quality metric in this section:

$$\mathrm{SSIM}(f,g) = \frac{(2\mu_f\mu_g + C_1)(\sigma_{fg} + C_2)}{(\mu_f^2 + \mu_g^2 + C_1)(\sigma_f^2 + \sigma_g^2 + C_2)} \tag{16}$$

where μ_f, σ_f^2 and σ_{fg} represent the mean of f, the variance of f, and the covariance of image f and g, respectively. C_1 and C_2 are small constants which eliminate unstable results when either $(\mu_f^2 + \mu_g^2)$ or $(\sigma_f^2 + \sigma_g^2)$ is very close to zero. The value of SSIM is mainly controlled by the structure similarity and varies from 0 to 1 which achieves its maximum value of 1 when the two images are exactly the same.

According to Eq. (11) and Eq. (12), the different choices of standard deviation σ of Gaussian filter result in different enhancement degrees to the basic denoised image. Figure 3 shows the effect of enhancement performances (without hard-threshold step) with different standard deviations in value of SSIM and PSNR.

Figure 3(a) illustrates that the value of SSIM rises with the increase of standard deviation of Gassian filter and becomes stable when standard deviation is larger than $\sigma = 1.9$. The performance of Figure 3(b) evaluated by PSNR goes the same way as Figure 3(a) which performs stably after $\sigma = 1.9$. Adopting

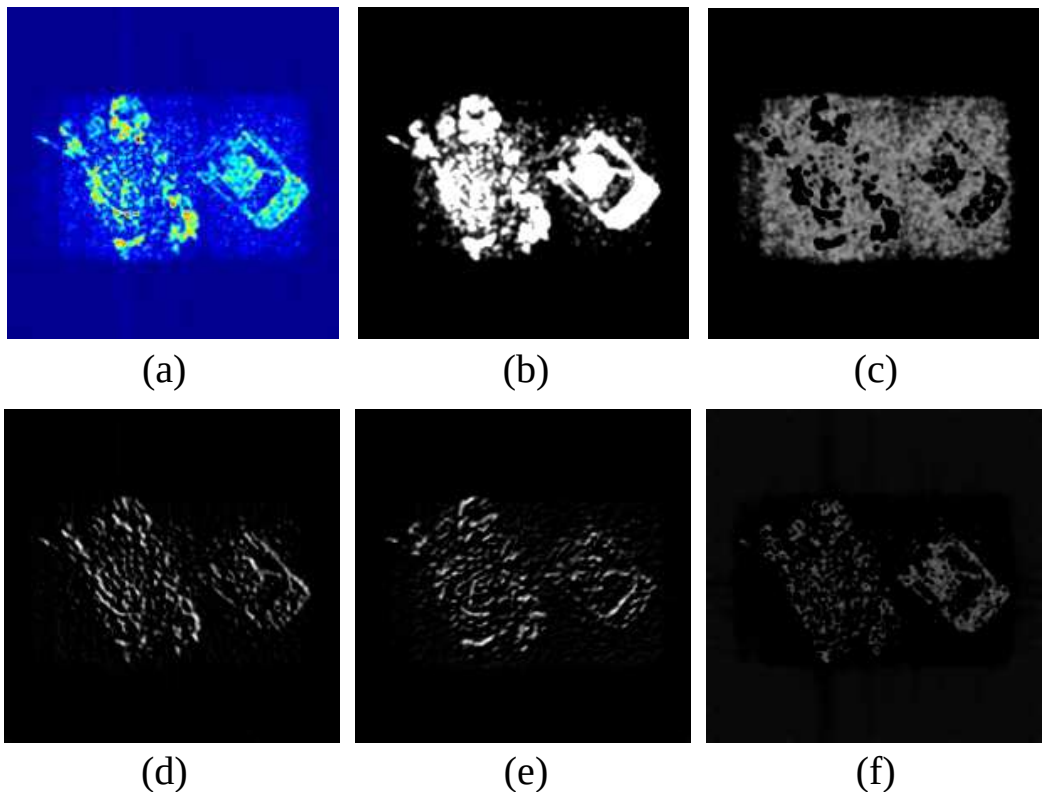

Figure 2. The first several dimensions of image data. (a) The input PMMW image, (b) first high-dimensional image data, (c) second high-dimensional image data (d) third high-dimensional image data (e) fourth high-dimensional image data, and (f) fifth high-dimensional image data.

small standard deviation ($\sigma < 1.0$), with enhancing the target edge comes an enhancement of the noise information as well. This makes the enhanced image perform badly in SSIM and PSNR. Although large standard deviation cannot bring strong enhancement to the target information, noise, as the main factor resulting in bad performance, is not enhanced. In addition, since overlarge σ brings excessiveness smooth phenomenon in Gaussian operator, the enhanced image becomes blurry (see Section 3) without improving much in SSIM and PSNR performance when σ is too large. Taking this phenomenon into account, we choose an acceptable default standard deviation parameter as: $\sigma = 1.9$.

The hard-threshold filtering step is used for filtering noise that had been enhanced in previous step, and the choice of hard-threshold also affects the final denoising performance of our algorithm. Figure 4 is the three dimensions of enhanced PMMW image, whose first dimension (Figure 4(b)) contains the main structure of the target, the second dimension (Figure 4(c)) describes the detail information, while the third dimension (Figure 4(d)) is mostly the noise and background information. Therefore, different hard-thresholds are adopted according to each dimension. To the first dimension, as it contains the main structure, filtering with the smallest threshold is adopted, and to the second dimension, filtering with the smaller one is applied and to the last dimension, zero operation to image data is performed to remove the background and noise information. The performance of hard-threshold filtering to with different hard-threshold δ is shown in Table 1.

According to Table 1, relatively large thresholds of first two dimensions bring better filtering performance which wipes away the noise embedded in structure and detail information. It is clear to see that the SSIM performances of three images leap suddenly when the first dimensional threshold $\delta_1 = 0.04$ goes to $\delta_1 = 0.05$ and remains stable after that. This phenomenon can be explained that the value of pixels (background noise) in the first dimension is too close that much noise can be filtered by suitable threshold without filtering the target information, which leads to a great improvement.

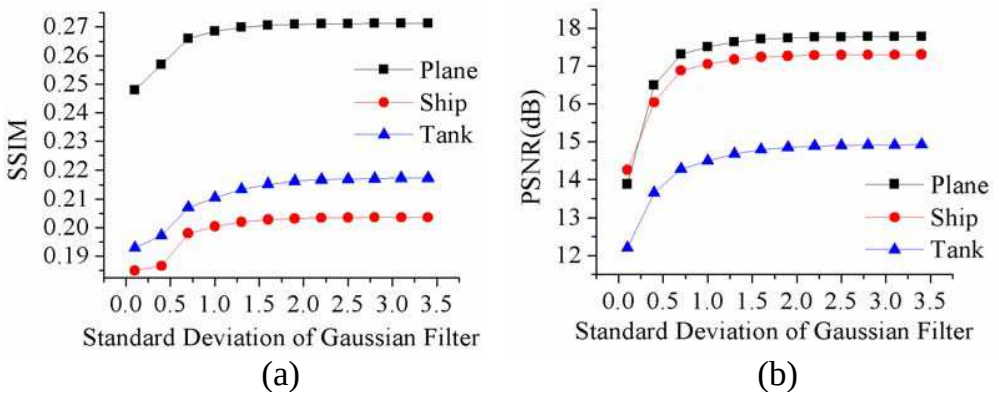

Figure 3. Enhancement performances (without hard-threshold step) in SSIM with different standard deviations of three simulate PMMW images.

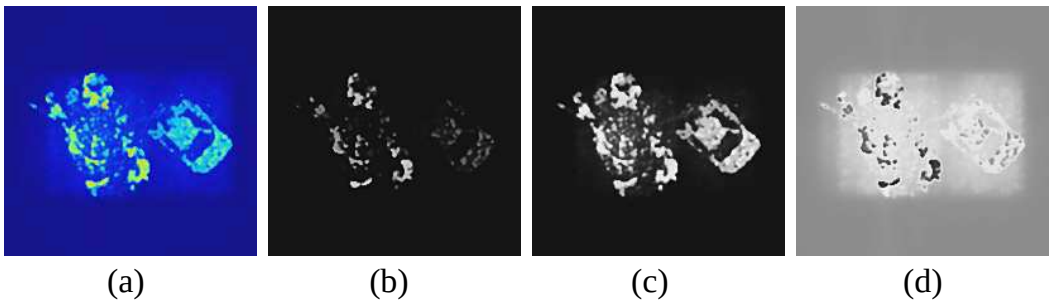

Figure 4. The three dimensions of enhanced image. (a) The result of image enhancement, (b) first dimension of enhanced image (c) second dimension of enhanced image, and (d) third dimension of enhanced image.

Table 1. Hard-threshold filtering performance with different hard-thresholds on two dimensions of PMMW image.

SSIM Performance		Threshold of filter δ_2 (2nd-D)											
		Tank				Plane				Ship			
		0.04	0.08	0.12	0.28	0.04	0.08	0.12	0.28	0.04	0.08	0.12	0.28
Threshold of filter δ_1 (1st-D)	0.03	0.410	0.745	0.758	0.752	0.494	0.788	0.801	0.800	0.494	0.788	0.801	0.799
	0.04	0.410	0.745	0.758	0.752	0.494	0.788	0.801	0.800	0.494	0.788	0.801	0.799
	0.05	0.546	0.863	0.874	0.864	0.615	0.844	0.851	0.842	0.615	0.845	0.851	0.842
	0.06	0.546	0.863	0.873	0.864	0.615	0.844	0.851	0.842	0.615	0.844	0.851	0.842
	0.07	0.546	0.863	0.873	0.864	0.615	0.844	0.851	0.842	0.615	0.844	0.851	0.842

For the second dimensional threshold, too large threshold ($\delta_2 > 0.28$) result in the loss of some detail information, while smaller threshold ($\delta_2 < 0.08$) lower down the filtering efficiency. It is found in the experiments that adopting threshold around $\delta_2 = 0.24$ are able to achieve a satisfactory performance both in SSIM and visual effect. Therefore $\delta_1 = 0.06$ and $\delta_2 = 0.24$ are chosen as the default threshold which works well and performs stably.

3. EXPERIMENTAL RESULTS AND DISCUSSIONS

In this section, the filtering results of adaptive manifolds filtering based on non-local means (AM-NLM) algorithm and our proposed one are displayed. And they are tested with default parameters with 6 PCA-computed retained dimensions for AM-NLM, and the other parameters discussed in Section 2.3 are adopted for the proposed algorithm. As we had analyzed, due to the spherical wave has serious influence on near range millimeter wave radiometer imaging, SSIM taking advantage of the comparison of structure to judging the similarity of two images, is used as main image quality metric. PSNR, as the supplementary one, is given as well. Table 2 presents the filtering performance of AM-NLM and the proposed method in SSIM and PSNR.

It is shown in the Table 2 that our proposed filtering algorithm achieves a great improvement in SSIM performance which looks unauthentic at first glance. As the value of SSIM mainly decided by structure comparison, our proposed method removes the rectangular noise produced by partial coherence between the point targets which affects the structure of the target in AM-NLM denoised

Table 2. Comparison of AM-NLM performance with the proposed method in terms of SSIM and PSNR.

	Method	Tank	Plane	Ship
SSIM	Simulated PMMW	0.275	0.321	0.271
	AM-NLM	0.280	0.326	0.273
	Proposed	0.866	0.845	0.920
PSNR (dB)	Simulated PMMW	15.169	18.737	18.208
	AM-NLM	15.612	19.663	18.734
	Proposed	15.248	21.024	18.559

image. The PSNR performance, as the supplementary objective image quality metric, stays at the same level compared with AM-NLM.

Figures 5, 6 and 7 display the filtering results of AM-NLM algorithm and the proposed one. AM-NLM works well on the PMMW image for which most of the noise can be filtered and the visual effect of the result (Figures 5(c), 6(c), and 7(c)) is also acceptable. However, the results of AM-NLM are a little bit blurry and the main target is not outstanding enough for some special engineering practice, such as target identification, crack detection and medical test. The results of our proposed algorithm (Figures 5(d), 6(d), and 7(d)) wipe off the useless background and noise information to make it easy to identify the target. What's more, the enhancement of the target edge makes it well distinguished. Therefore, our proposed PMMW filtering algorithm represents more outstanding and recognizable results, performing better in objective image quality metric and subjective visual effect.

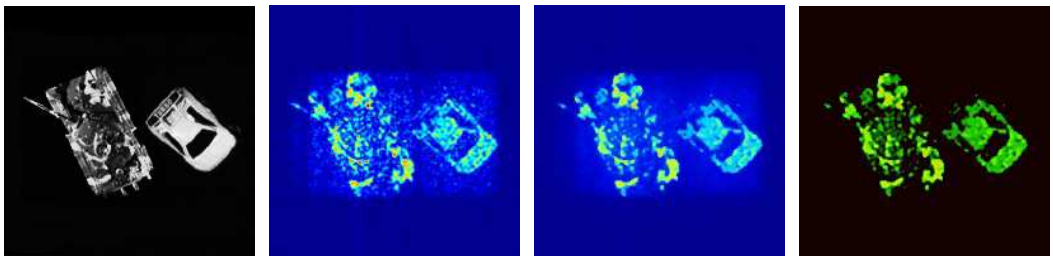

Figure 5. The comparison of filtering performance of AM-NLM and proposed algorithm of tank. (a) Target scene. (b) Simulated PMMW image. (c) Filtered by AM-NLM algorithm. (d) Filtered by our proposed algorithm.

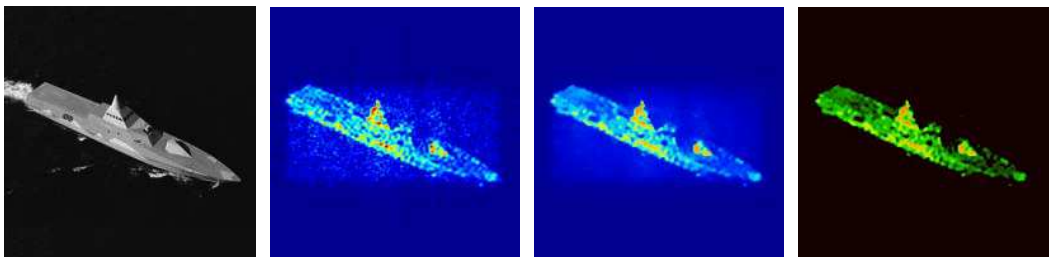

Figure 6. The comparison of filtering performance of AM-NLM and proposed algorithm of ship. (a) Target scene. (b) Simulated PMMW image. (c) Filtered by AM-NLM algorithm. (d) Filtered by our proposed algorithm.

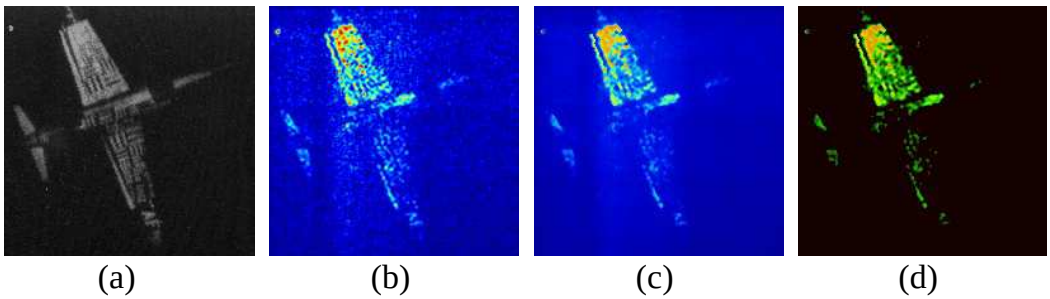

Figure 7. The comparison of filtering performance of AM-NLM and proposed algorithm of plane. (a) Target scene. (b) Simulated PMMW image. (c) Filtered by AM-NLM algorithm. (d) Filtered by our proposed algorithm.

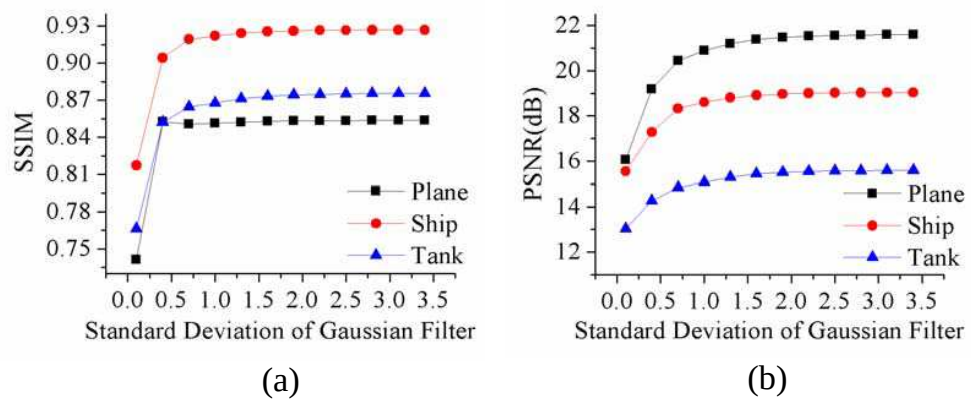

Figure 8. Final filtering performances in SSIM and PSNR using different standard deviations for the three simulated PMMW images.

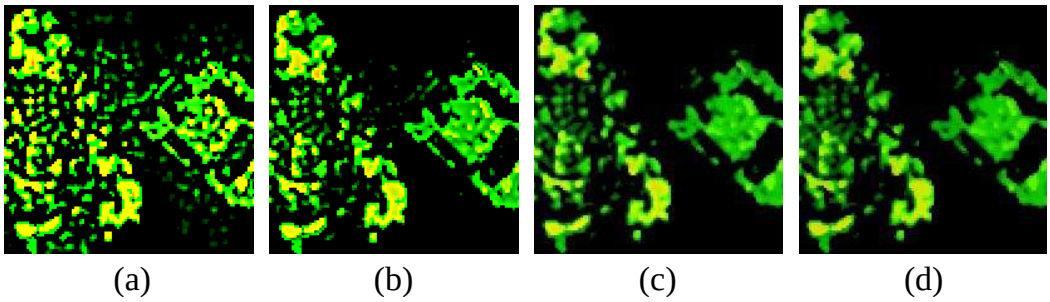

Figure 9. Enhancement performance of PMMW image with different standard deviations. (a) Enhanced by $\sigma = 0.2$ (SSIM = 0.825). (b) Enhanced by $\sigma = 0.5$ (SSIM = 0.859). (c) Enhanced by $\sigma = 1.9$ (SSIM = 0.866). (d) Enhanced by $\sigma = 4.0$ (SSIM = 0.867).

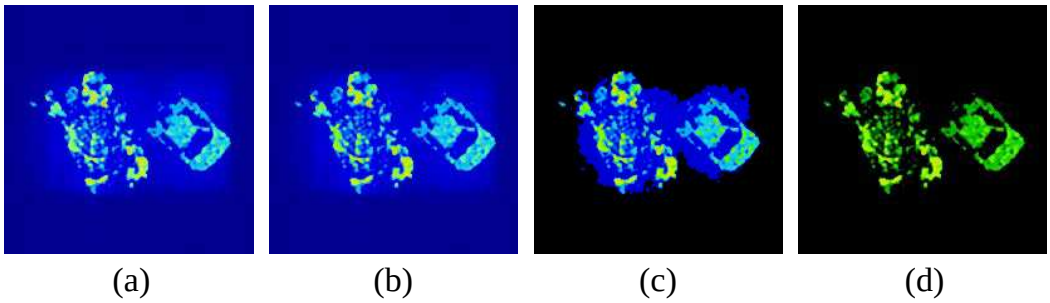

Figure 10. The comparison of denoising performance with different thresholds in third dimension. (a) Denoised by $\delta = 0.2$ (SSIM = 0.283). (b) Denoised by $\delta = 0.5$ (SSIM = 0.284). (c) Denoised by $\delta = 0.8$ (SSIM = 0.846). (d) Denoised by zero operation (SSIM = 0.866).

In order to test the correctness of the choice of parameters discussed in Section 2.3, adopting different standard deviations of Gaussian filter to the PMMW images and the corresponding results are shown in Figures 8, 9 and 10.

Figures 8(a) and (b) represent the final SSIM and PSNR performance affected by the various standard deviations. Compared with Figure 3, SSIM and PSNR in Figure 8 improve enormously which proves the effectiveness and necessity of hard-threshold filtering step. And it can also be seen from Figure 8 that the values of SSIM and PSNR vary almost the same way as in Figure 3 with the value

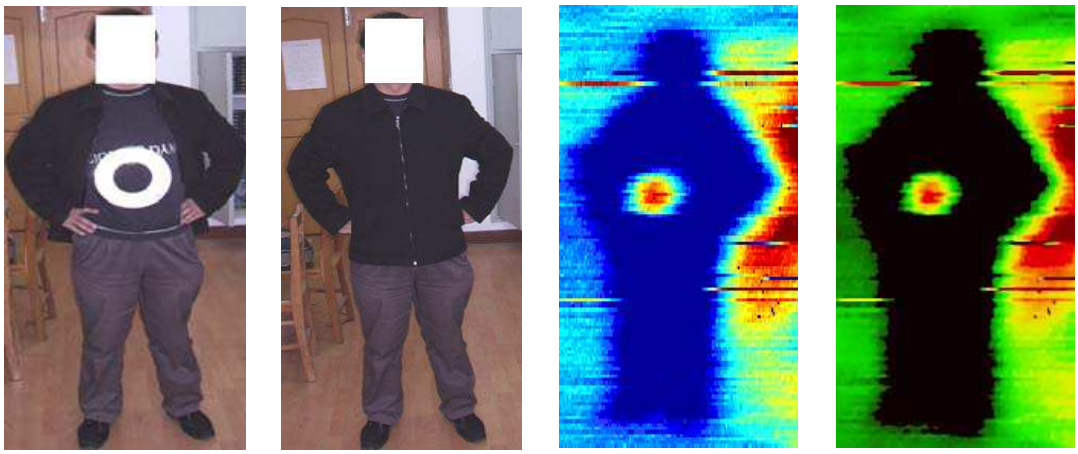

Figure 11. The filtering performance of proposed algorithm for real PMMW image. (a) Reference scene. (b) Target scene. (c) Real PMMW image. (d) Filtered by our proposed algorithm

growing gradually and arriving stable after $\sigma = 1.9$.

In addition, as shown in Figures 9(a) and (b), it is obvious that small standard deviation leads to the strong enhancement of the useless noise information although the detailed information of the target is enhanced as well. Meanwhile, the image with relatively large standard deviation ($\sigma = 4.0$) is more blurry than the formers and may lose some important detail information. Consequently, employing $\sigma = 1.9$ in image enhancement step is quite suitable in our proposed method which not only enhances the edge information without much noise, but also avoids bringing the blur to the image.

Figure 10 shows the denoising performance of the hard-threshold filtering on the third dimension with the default value of thresholds in other two dimensions that has been discussed in Section 2.3. As the noise has been enhanced in the image enhancement step, the third dimensional threshold adopted in Figures 10(a) and (b) can only filter mild noise. In Figure 10(c), most of the noise is filtered, but the strong ones located around the target are still retained. Figure 10(d) displays the result of zero operation which the background and noise information are almost completely wiped off. Consequently, do zero operation to the third dimension is workable which makes the target well distinguished.

To test the feasibility and efficiency of our proposed algorithm, we apply this method in real image system, and the filtering performance is displayed in Figure 11. It can be seen that our proposed algorithm is workable and satisfactory for real PMMW image. The mental ring in Figure 11(d) can be evidently extracted and well distinguished. Moreover, most of the noise and redundant information are eliminated.

4. CONCLUSIONS

In this paper, the adaptive manifolds filtering algorithm based on non-local means has been illustrated in detail, and an improved version of AM-NLM is proposed to denoise the simulate PMMW image. Our proposed algorithm takes the advantage of AM-NLM to gain a basic denoised PMMW image, and applies the image enhancement algorithm based on Laplacian of Gaussian operator to enhance the target edge. The hard-threshold filtering is adopted to gain the final denoised PMMW image.

The proposed PMMW image filtering algorithm can outline the structure of target and filter the disturbance, such as background and noise information. The parameters chosen in this paper can achieve a satisfactory result. The experiments show that our method performs better than AM-NLM in both objective image quality metric and objective visual effect. Meanwhile, we find that our proposed algorithm is also feasible for real PMMW image.

REFERENCES

1. Tuovinen, J., N. Hughes, P. Jukkala., P. Kangaslathti, T. Karttaavi, P. Sjoman, and J. Varis, "Technology for millimeter wave radiometers," *IEEE Transactions on Microwave Theory and Techniques*, Vol. 2, 883–886, 2003.
2. Bonafoni, S., F. Alimenti, G. Angelucci, and G. Tasselli, "Microwave radiometry imaging for forest fire detection: A simulation study," *Progress In Electromagnetics Research*, Vol. 112, 77–92, 2011.
3. Ruf, C. S., C. T. Swift, A. B. Tanner, and D. M. Le Vine, "Interferometric synthetic aperture microwave radiometry for the remote sensing of the earth," *IEEE Transactions on Geoscience and Remote Sensing*, Vol. 26, No. 5, 597–611, 1988.
4. Histace, A., *Image Restoration — Recent Advances and Applications*, InTech, Morn Hill, 2012.
5. Wang, B. and X. Li, "Near range millimeter wave radiometer passive image high resolution restoration," *IEEE Global Symposium on Milimeter Waves*, 325–328, 2008.
6. Reeves, S. J., "Analysis of the difficulties and possibilities for super-resolution," *Proc. SPIE*, Vol. 3064, 239–248, 1997.
7. Zheng, X. and J. Yang, "Adaptive projected landweber super-resolution algorithm for passive millimeter wave imaging," *Proc. SPIE*, Vol. 6787, 1001–1007, 2007.
8. Lucy, L. B., "An iteration technique for the rectification of observed distributions," *Astronomical Journal*, Vol. 79, 745, 1974.
9. Richardson, W. H., "Bayesian-based iterative method of image restoration," *Journal of the Optical Society of America*, Vol. 62, 55–59, 1972.
10. Hunt, B. R. and P. Sementilli, "Description of a poisson imagery super resolution algorithm," *Astronomical Data Analysis Software and Systems I*, Vol. 52, 196–799, 1992.
11. Li, L., J. Yang, G. Cui, J. Wu, Z. Jiang, and X. Zheng, "Super-resolution processing of passive millimeter wave image based on conjugate-gradient algorithm," *Journal of Systems Engineering and Electronics*, Vol. 20, No. 4, 762–767, 2009.
12. Xiao, Z., J. Xu, and S. Peng, "Super resolution image restoration of a PMMW sensor based on POCS algorithm," *Systems and Control in Aerospace and Astronautics*, 680–683, 2006.
13. Park, H., S. Kim, M. K. Singh, J. Choi, H. Lee, and Y. Kim, "Performance of wavelet based restoration for passive millimeter-wave images," *Proc. SPIE*, Vol. 5879, 157–166, 2005.
14. Zhang, Q., Y. Fu, L. Li, and J. Yang, "A millimeter-wave image denoising method bsed on adaptive sparse representation," *IEEE International Conference on Computational Problem-Solving*, 652–655, 2011.
15. Gastal, E. S. L. and M. M. Oliveira, "Adaptive manifolds for real-time high-dimensional filtering," *Proc. SIGGRAPH*, Vol. 31, No. 4, 33, 2012.
16. Tasdizen, T., "Principal components for non-local means image denoising," *IEEE International Conference on Image Processing*, 1728–1731, 2008.
17. Chen, J., Y. Li, J. Wang, Y. Li, and Y. Zhang, "An accurate imaging algorithm for millimeter wave synthetic aperture imaging radiometer in near-field", *Progress In Electromagnetics Research*, Vol. 141, 517–535, 2013.
18. Wang, Z. and E. P. Simoncelli, "Stimulus synthesis for efficient evaluation and refinement of perceptual image quality metrics," *Proc. SPIE*, Vol. 5292, 99–108, 2004.